

# An Alternative Method for a Reliable Estimation of Seismicity with an Application in Greece and the Surrounding Area

by C. Papazachos

**Abstract** An alternative method is proposed for the robust estimation of  $a$  and  $b$  values of the Gutenberg–Richter relation. The main hypothesis is that  $b$  values depend on material properties and the seismotectonic setting and therefore should vary relatively smoothly in space. As far as the  $a$  values are concerned, more sharp variations are allowed because these values determine the seismicity level, once the  $b$  value is fixed. The study area is organized into a grid, and the  $a$  and  $b$  values are simultaneously determined for the whole grid by solving an appropriate linear system. Smooth  $b$  variations are imposed by introducing additional linear constraints, similar to the Occam's inversion used in tomography studies. The method is applied to Greece and the surrounding area, which is a high seismicity area. The results are in very good agreement with previous studies and further enhance our knowledge for the study area. Moreover, additional seismicity measures (return periods, probabilities, etc.) are estimated robustly because they depend on the  $a$  and  $b$  values obtained for this area.

## Introduction

Research on quantitative studies of seismicity is usually oriented toward the solution of practical seismological problems, such as seismic hazard assessment, or toward the better understanding of geotectonic setting and active tectonics. Mean return periods or other relative quantities are currently used for seismic hazard assessment (Kaila and Narain, 1971; Rikitake, 1976; Singh *et al.*, 1981; Papazachos *et al.*, 1987, among others). The estimation of these quantities, as well as of other seismicity measures such as the rate of seismic energy or moment release (Makropoulos and Burton, 1983; Papazachos, 1990; Pacheco and Sykes, 1992), is usually based on the magnitude distribution parameters (Gutenberg and Richter, 1944), and hence, their reliable determination depends on the errors involved in the calculation of these parameters. Therefore, the accurate estimation of the Gutenberg–Richter parameters is important for any seismicity study. Although this estimation seems trivial, it is a difficult problem. Especially, the slope  $b$  is very sensitive to the size and quality of the available data sample (e.g., Papazachos, 1974).

The usual procedure is to compute the geographical distribution of seismicity by separating the examined area in small seismogenic subregions or cells and estimate  $a$  and  $b$  for each subregion or cell. However, the regionalization of seismicity measures cannot always be made objectively on the basis of these results due to the quantity and quality of the available data, neither can it be based only on the existing seismotectonic knowledge. For this reason, new techniques

are needed that incorporate both the existing seismological data and the current understanding about the specific seismotectonic setting in the area.

The purpose of the present work is to propose an alternative method for the estimation of  $a$  and  $b$  values. The underlying assumption is that the variation of  $b$  values depends on the seismotectonic setting of each subregion, and therefore, spatial correlation and small variations of the  $b$  value should be expected. For the values of the  $a$  parameter, a weaker spatial correlation is imposed because it reflects seismicity, which may change rapidly in space. The method is applied to study the geographical distribution of shallow seismicity in Greece and the surrounding area (34° N to 43° N, 18° E to 30° E), using a revised reliable catalog of historical and present-century events for this area (Papazachos *et al.*, 1997a).

## Problem Formulation

### Quantitative Estimates of Seismicity

The quantitative estimation of time-independent seismicity is usually based on the assumption of a Poisson time distribution and a Gutenberg–Richter (1944) frequency–magnitude relation, of the following form:

$$\log N_i = a_i - b M, \quad (1)$$

where  $N_i$  is the number of events with magnitude  $M$  or larger

that occurred in a  $t$ -years period of time within the examined seismogenic region covering a surface of  $S$  km<sup>2</sup>. Parameters  $a_t$  and  $b$  are determined from the data, provided that the data sample has certain properties (time homogeneity and completeness, accuracy, etc.). Reduction of equation (1) to unit time (1 year) and surface (1 km<sup>2</sup>) results in

$$\log N = a - b M, \quad (2)$$

where  $a = a_t - \log t - \log S$ . Once  $a$  and  $b$  are determined, the mean return period in an area of 1 km<sup>2</sup> for events with magnitude larger or equal to  $m$  is calculated by

$$T_m = 10^{bm}/10^a. \quad (3)$$

Assuming that a Poisson time distribution applies to seismicity, the probability,  $P_r$ , that an event with magnitude  $M$  or larger occurs in an area of 1 km<sup>2</sup> during a time period  $t$  is given (Lomnitz, 1974) by

$$P_r = 1 - \exp(-10^{a-bM} \cdot t). \quad (4)$$

Equations (3) and (4) are a typical example of the well-known importance of equation (2) for seismology. Various researchers have examined the variation of the  $b$  parameter and suggested significant spatial variations in different environments (e.g., Mori and Abercrombie, 1997; Wyss *et al.*, 1997). On the other hand, large-scale studies have shown little variation of the  $b$  value (Frolich and Davis, 1993).

One of the most problematic points in the  $b$ -value estimation is its sensitivity on the specific data set used. Papazachos (1974) demonstrated that false  $b$ -value variations (usually larger  $b$  values) can be found, if the magnitude range used for the determination of equation (1) is less than 1.5. Another typical example of false  $b$ -value variation concerns comparing two areas, which have exactly the same seismicity up to a certain magnitude, for example,  $M_{\min}$ , but only one of them has events with magnitudes between  $M_{\min}$  and a higher cut-off magnitude, for example,  $M_{\max}$ . Because equation (1) takes into account the cumulative number of earthquakes, these two areas will have different  $b$  values, as the additional earthquakes between  $M_{\min}$  and  $M_{\max}$  will change the slope of the log  $N$ - $M$  relation.

The previously mentioned problems in the  $b$ -value estimation suggest that much of the observed small-scale strong variability of the  $b$  value might be a result of numerical instabilities or data related problems and does not reflect true spatial variations. On the other hand, several authors have suggested that the  $b$  value depends on physical factors such as the heterogeneity of the material or the stress field in the focal region (Mogi, 1967; Scholz, 1968). For these reasons, it is natural to assume that the  $b$  value depends on the specific seismotectonic setting of each subregion, and therefore, it should exhibit smooth spatial variations. In the following, we formulate an appropriate method for retrieving such smooth  $b$ -value variations. Similar arguments are

used for the  $a$  parameter, although a much larger degree of spatial variation is allowed, in order to map the variation of seismicity in space.

### Method

From equations (3) and (4), it is clear that the reliable estimation of  $a$  and  $b$  parameters of equation (2) is crucial for any other seismicity parameter calculation. If we want to estimate the spatial distribution of these values, one possibility is to separate the area under study into smaller cells and perform a simple estimation of  $a$  and  $b$  for each cell. However, these estimates usually exhibit large errors due to the small number of available data, the small magnitude range spanned by the data, etc. On the other hand, increasing the cell size in order to obtain an adequate data set results in a loss of local information concerning the spacial distribution of seismicity.

In the present study, we propose a one-step estimation of spatial distribution of  $a$  and  $b$ . The examined area is divided into  $K$  cells (which might overlap), and using the completeness information for the whole data set, the complete data set for each cell is extracted, and the cumulative number of events,  $N$ , for each magnitude,  $M$ , is computed. Suppose that for each cell,  $i$ , a total number of  $n_i$  such pairs ( $[N_{ij}, M_{ij}]$ ,  $j = 1, \dots, n_i$ ) is found, where the  $i$  and  $j$  subscripts denote that this is the  $j$ th pair belonging to cell  $i$ . If  $a_i$  and  $b_i$  are the Gutenberg–Richter parameters for each cell, the following relation holds:

$$\log N_{ij} = a_i + b_i M_{ij} = \sum_{k=1}^K \delta_{ik}(a_k + b_k M_{kj}) \quad (5a)$$

$$(i = 1, \dots, K, j = 1, \dots, n_i),$$

where  $\delta_{ik}$  is the Kronecker delta.

Equation (5a) is written in such a way so that all the unknowns appear in each equation, forming the following linear system:

$$\mathbf{N} = \mathbf{A} \begin{bmatrix} \mathbf{a} \\ \mathbf{b} \end{bmatrix} = \mathbf{A}\mathbf{x}, \quad (5b)$$

where  $\mathbf{N}$  contains the log  $N_{ij}$  values,  $\mathbf{a}$  and  $\mathbf{b}$  are vectors containing the  $a_i$  and  $b_i$  values ( $i = 1, \dots, K$ ) for all cells, respectively,  $\mathbf{x}$  is the combined vector of  $\mathbf{a}$  and  $\mathbf{b}$ , and matrix  $\mathbf{A}$  connects  $\mathbf{a}$  and  $\mathbf{b}$  with  $\mathbf{N}$ . Since equations (5a) are not coupled for different cells, the solution of the linear system is the same as the independent solution for each cell. In this study, we modify the linear system (5b) assuming that the  $b$  value depends mainly on material properties and the seismotectonic setting. Therefore, it is expected to vary slowly in space and to have similar values in neighboring cells. For this reason, additional constraints of the form

$$\lambda \partial^2 \mathbf{b} = 0 \quad (6)$$

are added to system (5b). Equation (6) imposes a smoothness constraint between neighboring cells, in a way similar to Occam's inversion (Constable *et al.*, 1987). The constant  $\lambda$  regulates the strength of these constraints. On the other hand, once the  $b$  values are fixed, the  $a_i$  ( $i = 1, \dots, N$ ) values determine the seismicity in each cell, which might vary significantly within small distances. For this reason, a similar equation can be applied to all  $a_i$  values:

$$\mu \partial^2 \mathbf{a} = 0 \quad (7)$$

but with  $\mu < \lambda$  in order to avoid the significant "spreading" from high to low seismicity areas and vice-versa.

However, we still have a problem with certain cells where very few data are available, even if smoothing is imposed through equation (7), since the estimation of  $a_i$  is subject to large errors. This is especially important for cells where the number of data is small but for which only large events are available. In such a case, once the  $b_i$  value is determined, the determination of  $a_i$  is subject to large errors, for example, if a single observation of a large event is available, it will lead to an erroneous large  $a_i$  value, because smaller events are not available. For those cases where very few observations of large events are available, we need to reduce the value of  $a_i$  as the uncertainty for its estimation is very large. According to Franklin (1970), this stabilization of the final solution is achieved by considering additional "damping" constraints of the form

$$\nu \tilde{\mathbf{a}} = 0. \quad (8)$$

The effect of these constraints is to reduce the  $a_i$  values when very few observations are available. In order to use such constraints only for cells with few data, equation (8) can be applied when the number of available data in a cell is smaller than a certain value  $n_{\text{cut}}$ . Therefore,  $\tilde{\mathbf{a}}$  in equation (8) contains only cells with  $n_i < n_{\text{cut}}$ . An alternative is to reduce the degree of damping (e.g., linearly) as the number of observations increases to  $n_{\text{cut}}$ ; hence, modify equation (8) to

$$\nu \left( 1 - \frac{n}{n_{\text{cut}}} \right) \tilde{\mathbf{a}}_n = 0 \quad (n = 0, \dots, n_{\text{cut}} - 1), \quad (9)$$

where  $\tilde{\mathbf{a}}_n$  corresponds to cells with  $n < n_{\text{cut}}$  observations.

Equations (5b), (6), (7), and (8) (or 9) define our final linear system. In order to obtain a maximum-likelihood estimation of  $\mathbf{a}$  and  $\mathbf{b}$ , these equations should be scaled to their *a priori* uncertainties, which can be incorporated in the form of an *a priori* covariance matrix, leading to the following system:

$$\begin{aligned} \mathbf{C}_N^{-1/2} \mathbf{N} &= \mathbf{C}_N^{-1/2} \mathbf{A} \mathbf{x}, \\ \lambda \partial^2 [\mathbf{C}_b^{-1/2} \mathbf{b}] &= 0, \\ \mu \partial^2 [\mathbf{C}_a^{-1/2} \mathbf{a}] &= 0, \\ \nu [\mathbf{C}_a^{-1/2} \tilde{\mathbf{a}}] &= 0, \end{aligned} \quad (10)$$

where  $\mathbf{C}_N$ ,  $\mathbf{C}_b$ , and  $\mathbf{C}_a$  are the *a priori* covariance matrices that correspond to vectors  $\mathbf{N}$ ,  $\mathbf{b}$ , and  $\mathbf{a}$ , respectively. Usually, in the absence of additional information, these covariance matrices are considered to be diagonal with the value of the expected variance as the diagonal value. After this rescaling of system (5b), equation (10) can be solved using standard least squares, leading to a maximum likelihood solution. The  $a_i$  and  $b_i$  estimation is now coupled through the additional constraints (6), (7), and (8) (or 9). Of course, the values of  $\lambda$ ,  $\mu$ , and  $\nu$  can be modified in order to regulate the amount of smoothing or damping imposed on our final results, similarly to the approach taken in inversion of linear systems for tomographic purposes, etc. Moreover, a possible alternative is to solve system (5b) using constraints (6) to determine  $\mathbf{b}$  (ignoring  $\mathbf{a}$ ) and then to resolve it using the constraints (7) and (8) (or 9) in order to determine  $\mathbf{a}$ , once  $\mathbf{b}$  is fixed. This second approach will reduce the strong coupling usually observed in estimations of  $a$  and  $b$ , although some coupling will still be present.

## A Case Study: Greece and the Surrounding Area

### A Reliable Data Sample for Shallow Seismicity in Greece and the Surrounding Area

Seismicity in the area of Greece is the highest in the whole western Eurasia, with mainly shallow ( $h \leq 40$  km) events and intermediate-depth events along the southern Aegean subduction (Fig. 1). Quantitative seismicity studies have been performed during the last three decades using instrumental data and both methods, which are based either on seismic energy release and relative quantities (Delibasis and

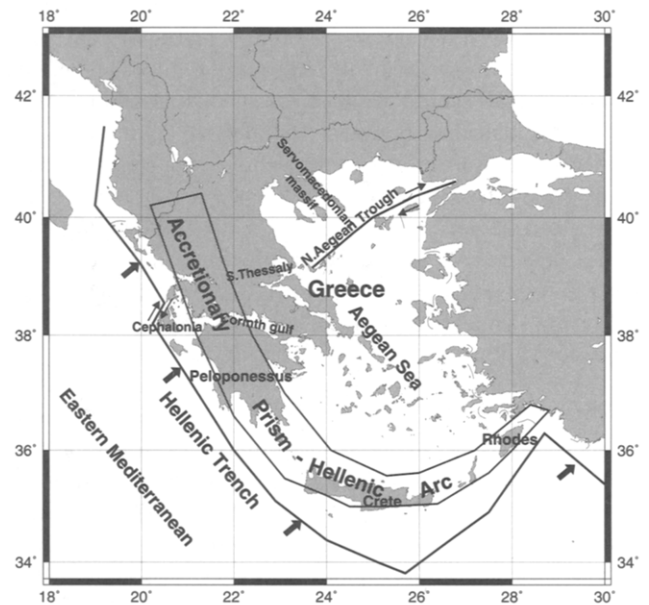


Figure 1. General seismotectonic features of the area under study.

Galanopoulos, 1965; Galanopoulos, 1972; Papazachos, 1990) or on the mean return period and similar seismicity measures (Comninakis, 1975; Makropoulos and Burton, 1984, 1985; Stavrakakis and Tselentis, 1987; Papazachos, 1990; Hatzidimitriou *et al.*, 1994).

Recently, a new improved earthquake catalog has been published (Papazachos *et al.*, 1997a) for the period 550 B.C. to 1995 A.D. A large part of the catalog is appropriate for a detailed study of the geographical distribution of shallow seismicity and is complete for the whole area under study for the following periods: After 1501 for  $M \geq 7.3$ , 1845 for  $M \geq 6.5$ , 1911 for  $M \geq 5.5$ , 1950 for  $M \geq 5.0$ , and 1970 for  $M \geq 4.5$ . All magnitudes are originally calculated or converted to the moment magnitude scale with a typical error of  $\pm 0.3$  (Papazachos *et al.*, 1997b) and a location error that does not exceed 30 km. Hence, this catalog was considered as an appropriate data sample for a verification of the method previously proposed. This complete data set is shown in Figure 2. Moreover, two additional events (365 A.D.,  $M = 8.3$ ; 1303,  $M = 8.0$ ) are also plotted in this figure. It is very probable that these two events also form a complete data set because such large events ( $M \geq 8.0$ ) have a very large impact, and historical (literal) information are always available.

In order to reduce the catalog to a homogeneous and complete data set, the observed cumulative frequencies are reduced to the same time period (Milne and Davenport, 1969). Figure 3 shows the logarithm of the cumulative observed frequency of earthquakes as a function of the moment magnitude, reduced to the whole historical period (550 B.C. to 1995). The six different completeness periods have been denoted by different symbols. A surprising result is that there seems to be a lack of large events ( $M \geq 7.0$ ) by approximately a factor of 2. The average  $b$  value for  $M \leq 7.0$  is  $b \approx -1.0$ . This slope change can be qualitatively explained as shown in the inner figure: Even if all subregions and seismic sources had the same  $b$  values, the maximum magnitude for each source would be different. If this maximum magnitude,  $M_{\max}$ , varies between  $M_1$  and  $M_3$ , then the superposition of the seismicity data for all seismic sources would result in a figure similar to the obtained  $\log N$ - $M$  curve for Greece and the surrounding area. However, this interpretation is very preliminary, and additional work needs to be made concerning the distribution of maximum magnitudes before final conclusions can be reached about the distribution observed in Figure 3.

### Results and Discussion

In order to test the applicability of the method, we initially used the data set for the period 1911 to 1995, because after 1911, all epicenters in Greece and the surrounding area were estimated from instrumental recordings. Using this data set, the final linear system (equations 10) was created. The number of  $[\log N_i, M_i]$  pairs used was 1494. Equations (5) and (6) were solved first in order to determine a smooth geographical distribution of  $b$ , by dividing the whole area in

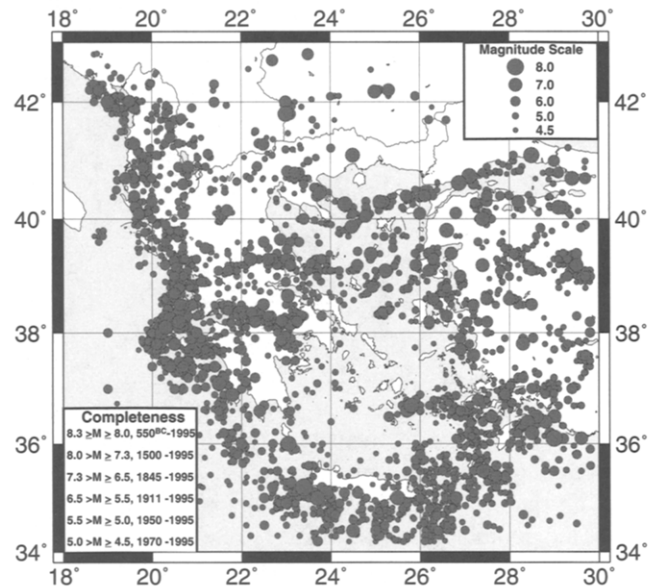


Figure 2. Epicenter map of six complete sets of shallow earthquakes in Greece and surrounding area. The magnitude scale and the completeness periods for which data were used are also shown.

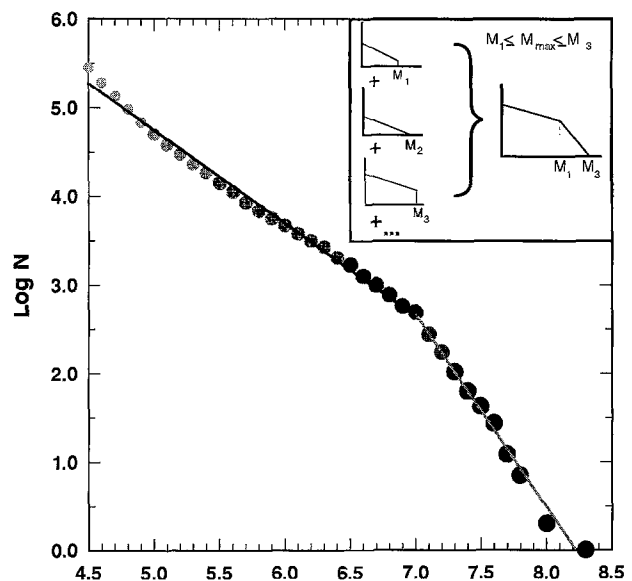


Figure 3. Plot of the cumulative number of observed earthquakes versus magnitude for the study area. All observational frequencies are reduced to the total time period studied (550 B.C. to 1995). Notice the slope change around  $M = 7.0$ , which is attributed to the maximum magnitude saturation for individual seismic sources (see inset figure and text for explanations).

a crude grid of nonoverlapping cells of  $0.5^\circ \times 0.5^\circ$ . The final results for the  $b$ -value distribution in Greece and the surrounding area have a data misfit of  $\sigma_{\log N}$  of 0.19 and are shown in Figure 4a. The results presented were obtained after scaling the  $b$  and  $\log N_i$  values and their *a priori* uncertainty,  $\sigma_b$  and  $\sigma_{\log N}$ , which was taken to be equal to 0.1 and 0.2 from previous studies (Hatzidimitriou *et al.*, 1985, 1994), and using an equal amount of misfit reduction and smoothing ( $\lambda = 1$ ).

The obtained pattern for the  $b$  values showed very little variation for a wide range of  $\lambda$  values. Figure 4b shows the results determined for the same data set using a smoothing reduced by 50% ( $\lambda = 0.5$ ). The obtained  $b$ -value distribution is almost identical to the distribution shown in Figure 4a. Moreover, in order to test the effect of historical seismicity, we incorporated the previously described data set of Papa-

zachos *et al.* (1997a) for the period 1501 to 1995. Although this data set resulted into only approximately 200 additional constraints ( $[\log N_i, M_i]$  pairs), the incorporation of historical data is important because more large earthquakes are included in the determination of  $b$ . The obtained results are shown in Figure 4c. Again, a very compatible distribution with the one presented in Figure 4a is seen, which demonstrates the robustness of the  $b$  values estimation even for this mixed historical-instrumental data set. For this reason, the distribution of Figure 4a is considered as final and is adopted for all further estimations.

The general pattern of the  $b$ -value spatial variation seen in Figure 4a correlates very well with the structure of the Hellenic arc (Fig. 1). A significant reduction of  $b$  values is observed as we move from the outer arc ( $b \approx 1.0$  to 1.1) to the back-arc area ( $b \approx 0.9$  to 0.7). This practically means

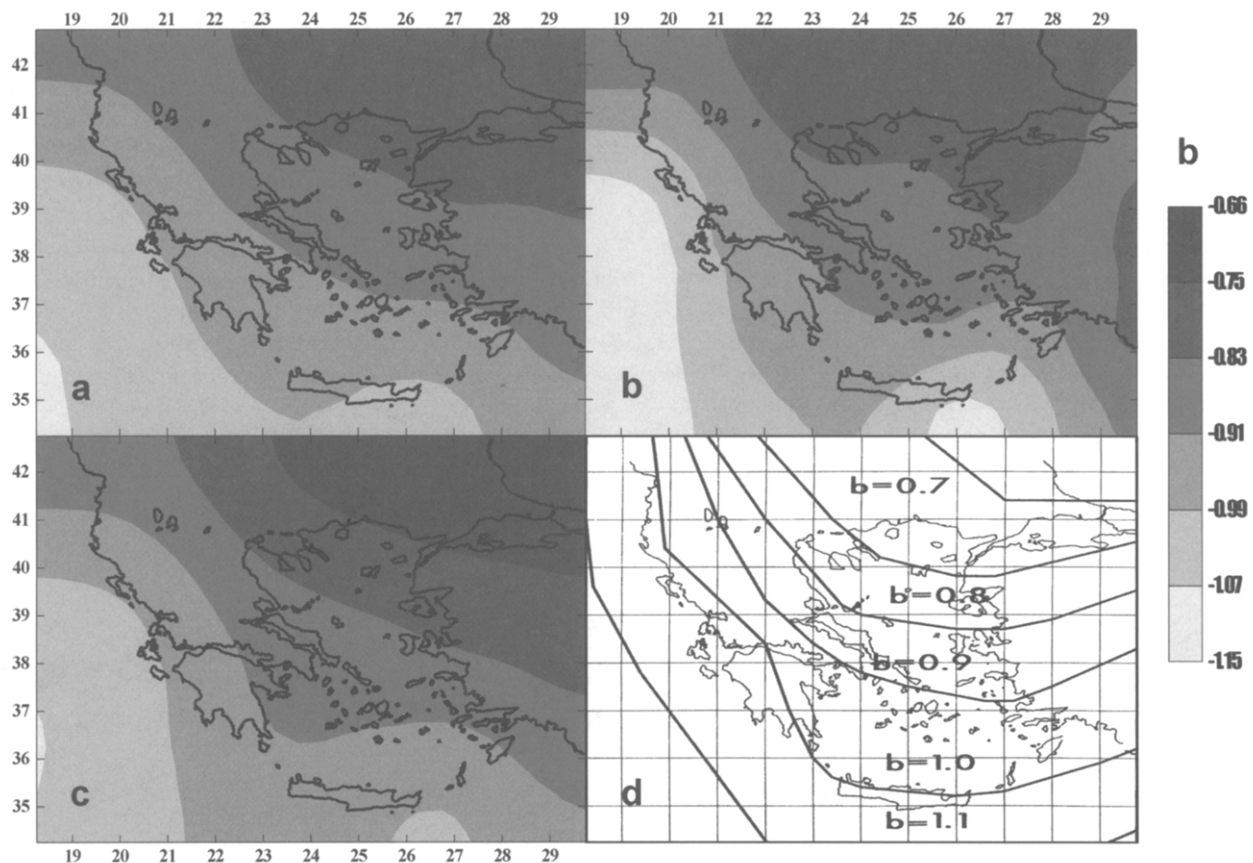


Figure 4. Geographical distribution of the  $b$  value in Greece and the surrounding area. (a) Results obtained using data for the period 1911 to 1995 for which instrumental data were available. (b) Same as (a) using a smoothing reduced by 50% (see text). (c) Distribution of  $b$  value when historical data from 1501 are also included in the data set. (d) Same results determined by Hatzidimitriou *et al.* (1994) obtained using standard seismogenic zonation and data for the period 1800 to 1992. A very good correlation is observed between all figures, showing the compatibility of the obtained results with standard methods as well as its stability to different data sets and spatial smoothing criteria. In general, an excellent correlation is observed between the resulting figure and the general features of the study area (Fig. 1), with higher  $b$  values (more small than large-magnitude events) for the outer-arc (collision-subduction) than for the back-arc area.

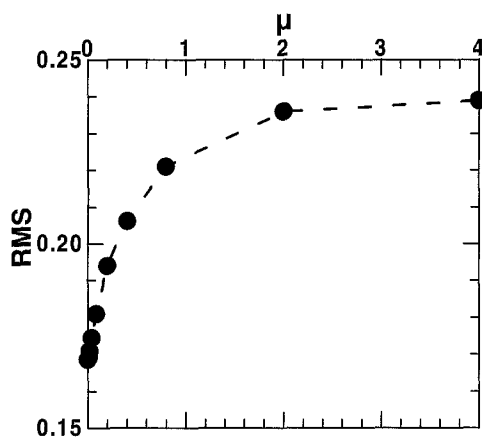


Figure 5. Plot of the rms misfit of the 4160  $[\log N_i, M_i]$  data used in the present study against the smoothing constant,  $\mu$ , used for the estimation of the  $a$  value for Greece and the surrounding area. Low  $\mu$  values correspond to a reduced smoothing while high  $\mu$  values result in strongly smoothed  $a$ -value distributions. An expected increase of the rms misfit with  $\mu$  is observed due to the bias introduced by the smoothing constraints for the  $a$ -value estimation.

that relatively more small-magnitude events occur in the outer arc where the Eastern Mediterranean–Aegean collision occurs and which is dominated by thrust faults, than in the back-arc area where normal and strike-slip faults are observed. This pattern is in very good agreement with the results of previous studies, which generalized the results of small-scale studies using traditional techniques. In Figure 4d, the results from Hatzidimitriou *et al.* (1994) are presented for comparison. This figure presents a smoothed dis-

tribution of the  $b$  values determined for various seismogenic zones (Papazachos and Papaioannou, 1993) using data for the period 1800 to 1992. The presented distribution is almost identical with the results presented here (Fig. 4a), which indicates the compatibility of the method proposed in this article with standard techniques.

Once  $b$  has been determined, the variation of  $a$  values corresponds to the variation of low-magnitude seismicity. In order to map smaller scale seismicity variations, the area was divided into smaller cells ( $0.25^\circ \times 0.25^\circ$ ) with 50% overlapping, and the complete data set (550 B.C. to 1995) was used, which resulted in 4160 constraints ( $[\log N_i, M_i]$  pairs). Because the number of unknowns (1645) and the number of data (4160) were quite large, the linear system (10) was solved much faster with a large matrix solver, which for our case was LSQR (Paige and Saunders, 1982). LSQR iterations were performed until no misfit reduction was observed, which leads to a solution identical to the least-squares solution (Paige and Saunders, 1982).

The value of  $\nu$  was set to 1 (similarly to  $\lambda$ ) after scaling the  $\mathbf{a}$  vector to its *a priori* error, which was taken to be equal to 0.4 from previous studies. For the smoothing parameter,  $\mu$ , a large set of values was examined, and the rms misfit of system (10) was examined. Figure 5 shows the variation of this rms misfit against  $\mu$ . Low  $\mu$  values correspond to less smooth distributions of  $\mathbf{a}$  and small rms misfits, while high  $\mu$  values lead to a more smooth spatial distribution but introduce more bias to the final solution, hence leading to higher rms values. It is observed that although the rms misfit increases quite rapidly for small  $\mu$  values, after a certain smoothing value ( $\mu \sim 2$ ), the solution has an almost constant misfit. In order to examine the possible limits of the distribution of the  $a$  value, results are presented for two  $\mu$  values

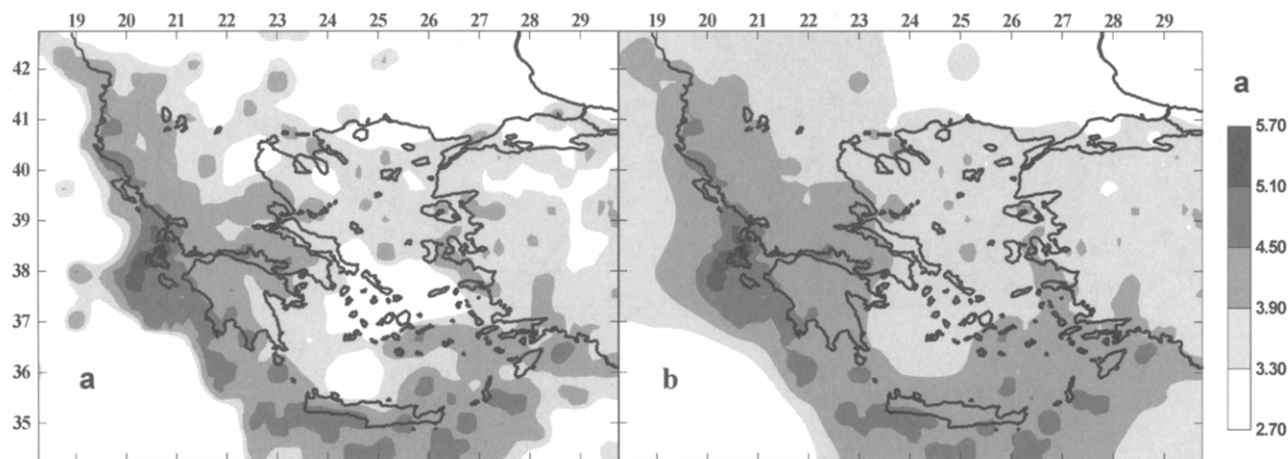


Figure 6. Geographical distribution of the  $a$  values normalized to 1 year and 10,000  $\text{km}^2$  for Greece and the surrounding area, using (a) low ( $\mu = 0.2$ ) and (b) high ( $\mu = 2$ ) smoothing constraints (see text for explanation). The two figures can be considered to provide the possible range for the  $a$ -value in each area. Although a general decrease of  $a$  values toward the NE is observed, a lot of small- and large-scale high seismicity areas (Corinth gulf, Southern Thessaly area, outer Hellenic arc, etc.) are also recognized.

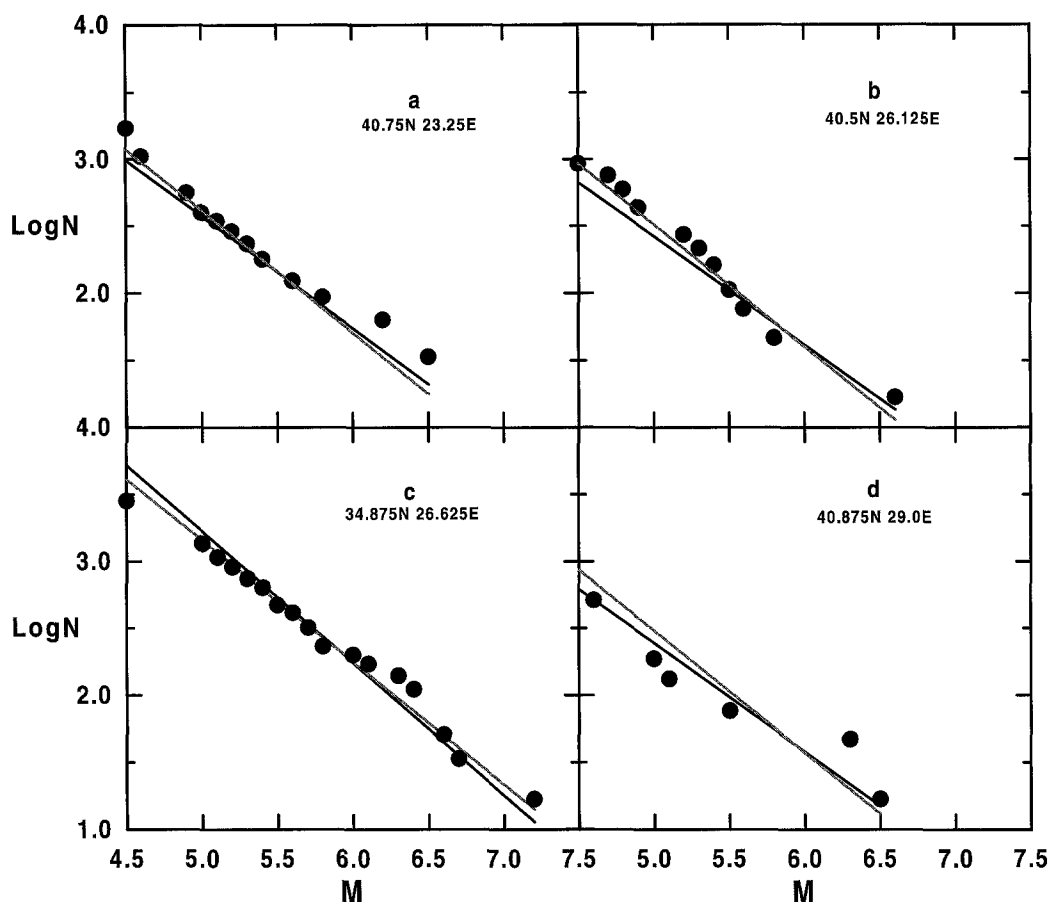


Figure 7. Comparison of the predicted Gutenberg–Richter curves (solid lines) with observed data (solid circles) for selected subregions of Greece and the surrounding area. The best-fit Gutenberg–Richter curves using a constant slope of  $b = 0.91$  (average  $b$ ) are also shown (gray lines). A very good correlation of the predicted and observed behavior of the  $\log N$ – $M$  distribution is observed. Moreover, the constant  $b$  value exhibits a poorer fit for some subregions (e.g., for  $d$ ).

equal to 0.2 and 2. The first  $\mu$  value ( $=0.2$ ) corresponds to a quite crude solution, while the second  $\mu$  value ( $=2$ ) was chosen in order to represent a smooth version of the  $a$ -value distribution, since the rms misfit practically does not change for  $\mu \geq 2$ . The final results were corrected for the slightly different surface of each cell and were reduced to a surface of 10,000 km<sup>2</sup> and a time period of 1 year.

The final map showing the distribution of the  $a$  value in Greece and the surrounding area is shown in Figure 6a for  $\mu = 0.2$  and Figure 6b for  $\mu = 2$ . The two distributions can be considered as describing the possible upper and lower limits for each site. Because the  $b$  value varies very slowly in space, several seismogenic sources can be identified from the distribution of  $a$  values, like the outer Hellenic arc (see Fig. 1). Moreover, a general tendency for  $a$  to decrease toward the NE is observed. However, because  $a$  measures only the low-magnitude seismicity, this general tendency is not also valid for the seismic energy release, as the  $b$  values also vary toward the NE (Fig. 4). For this reason, a detailed study of the spatial distribution of seismicity requires that proba-

bility maps (or mean return periods, etc.) are presented for several magnitude ranges.

Figure 7 shows a comparison between the determined Gutenberg–Richter curves (solid lines) and the available data for four well-sampled subregions in the examined area. For these subregions, the  $a$  values from Figures 6a and 6b were very close (due to the large number of data available), and their average value was used in Figure 7. In the same figure, the Gutenberg–Richter curves that were determined using a constant  $b$  value, equal to the average value determined for the study area ( $=0.91$ ), are also shown (gray lines). In general, a very good fit is observed between the data and the predicted curves. Moreover, although  $b$  does not show a very large variation, it is clear that the constant  $b$  value is not appropriate for some areas (e.g., Fig. 6d).

Of special interest is the map of the mean return periods for earthquakes with  $M \geq 6.0$ ,  $T_{6.0}$ , as these events usually cause significant damage in the examined area. In Figure 8, the geographical distribution of mean return periods for these events is presented for both maps presented in Figure

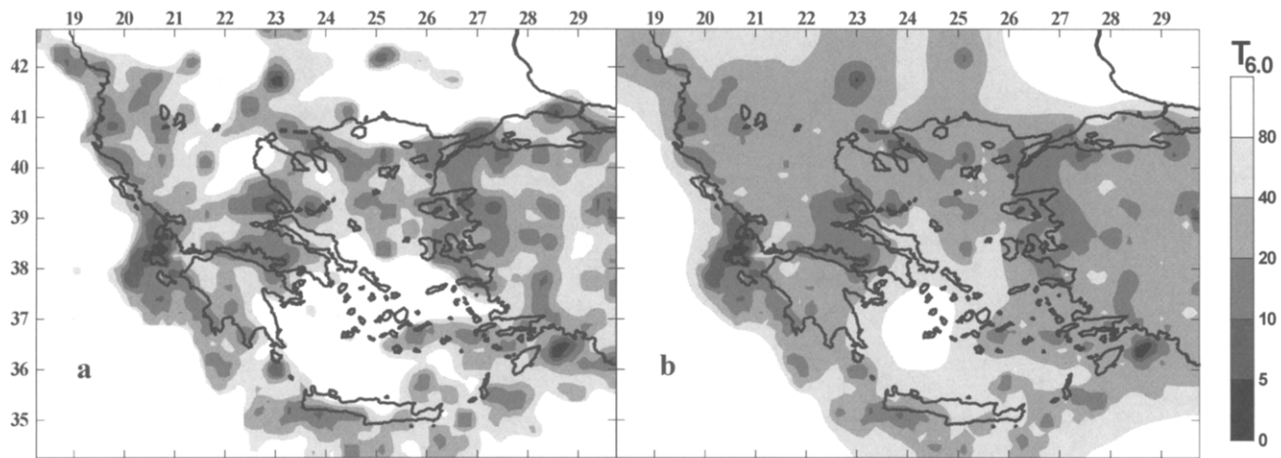


Figure 8. Geographical distribution of the mean return period of shallow earthquakes in Greece and the surrounding area for  $M \geq 6.0$  and per 10,000 km<sup>2</sup>, using the  $b$ -value distribution presented in Figure 4a and the  $a$ -value distribution of (a) Figure 6a and (b) Figure 6b. The high seismicity areas observed in Figure 6 are more clearly recognized in this figure.

6. The general pattern of seismicity given by the proposed method is in agreement with previous results; for example, the highest shallow seismicity is observed in the Cephalonia island (also seen in Fig. 7c). Moreover, additional detailed information is recognized, which does not depend on the subjective criteria of each observer. Clearly, delineated seismogenic volumes can be identified, especially in Figure 8a. The whole outer Hellenic arc exhibits small return periods (2 to 20 years), similarly to other high seismicity areas (Corinth gulf, southern Thessaly, Servomacedonian massif, northern Aegean, eastern Greek islands, and western coasts of Turkey). On the other hand, certain areas exhibit very large return periods (e.g., western Macedonia), in agreement with previous large-scale seismicity studies in the Aegean area (e.g., Papazachos, 1990).

### Acknowledgments

The author would like to thank Prof. B. Papazachos for his critical reading of the manuscript and valuable suggestions. This research has been partly funded by the PEP program (Project 7454 R.C. Univ. Thessaloniki) of the District of Central Macedonia (N. Greece).

### References

- Cominakis, P. E. (1975). Contribution to the study of the seismicity of Greece, *Ph.D. Thesis*, Univ. of Athens, 110 pp.
- Constable, S. C., R. L., Parker, and C. Constable (1987). Occam's inversion: a practical algorithm for generating smooth models from electromagnetic sounding data, *Geophysics* **52**, 289–300.
- Delibasis, N. and A. G. Galanopoulos (1965). Space and time variations of strain release in the area of Greece, *Am. Geol. Pays Helleniques* **18**, 135–146.
- Franklin, J. N. (1970). Well-posed stochastic extensions to ill-posed problems, *J. Math. Anal. Appl.* **31**, 682–716.
- Frohlich, C. and S. Davis (1993). Teleseismic  $b$ -values: or, much ado about 1.0, *J. Geophys. Res.* **98**, 631–644.
- Galanopoulos, A. G. (1972). Annual and maximum possible strain accumulation in the major area of Greece, *Ann. Geol. Pays Helleniques* **24**, 467–480.
- Gutenberg, B. and C. F. Richter (1944). Frequency of earthquakes in California, *Bull. Seism. Soc. Am.* **34**, 185–188.
- Hatzidimitriou, P. M., E. E. Papadimitriou, D. M. Mountrakis, and B. C. Papazachos (1985). The seismic parameter  $b$  of the frequency magnitude relation and its association with the geological zones in the area of Greece, *Tectonophysics* **120**, 141–151.
- Hatzidimitriou, P. M., B. C. Papazachos, and G. F. Karakaisis (1994). Quantitative seismicity of the Aegean and surrounding area, *Proc. of the XXIV Gen. Assembly of E.S.C.*, Athens, 19–24 September 1994, 155–164.
- Kaila, K. L. and H. Narain (1971). A new approach for preparation of quantitative seismicity maps as applied to Alpidic belt-Sunda arc and adjoin areas, *Bull. Seism. Soc. Am.* **61**, 1275–1291.
- Lomnitz, C. (1974). *Global Tectonics and Earthquake Risk*, Elsevier, Amsterdam, 320 pp.
- Makropoulos, K. C. and P. W. Burton (1983). Seismic risk of circum-Pacific earthquakes: 1) Strain energy release, *Pure Appl. Geophys.* **121**, 247–267.
- Makropoulos, K. C. and P. W. Burton (1984). Greek tectonics and seismicity, *Tectonophysics* **106**, 275–304.
- Makropoulos, K. C. and P. W. Burton (1985). Seismic hazard in Greece: 1) Magnitude recurrence, *Tectonophysics* **117**, 205–257.
- Milne, W. G. and A. G. Davenport (1969). Determination of earthquake risk in Canada, *Bull. Seism. Soc. Am.* **59**, 729–754.
- Mogi, K. (1967). Earthquakes and fractures, *Tectonophysics* **5**, 35–55.
- Mori, J. and R. E. Abercrombie (1997). Depth dependence of earthquake frequency-magnitude distributions in California: implications for the rupture initiation, *J. Geophys. Res.* **102**, 15081–15090.
- Pacheco, J. F. and L. R. Sykes (1992). Seismic moment catalog of large shallow earthquakes, 1900 to 1989, *Bull. Seism. Soc. Am.* **82**, 1306–1349.
- Paige, C. C. and M. A. Saunders (1982). LSQR: an algorithm for sparse linear equations and sparse least squares, *ACM Trans. Math. Software* **8**, 43–71.
- Papazachos, B. C. (1974). Dependence of the seismic parameter  $b$  on the magnitude range, *Pure Appl. Geophys.* **112**, 1059–1065.
- Papazachos, B. C. (1990). Seismicity of the Aegean and surrounding area, *Tectonophysics* **178**, 287–308.

- Papazachos, B. C. and Ch. Papaioannou (1993). Long-term earthquake prediction in the Aegean area based on a time and magnitude predictable model, *Pure Appl. Geophys.* **40**, 593–612.
- Papazachos, B. C., E. E. Papadimitriou, A. A. Kiratzi, Ch. A. Papaioannou, and G. F. Karakaisis (1987). Probabilities of occurrence of large earthquakes in the Aegean and surrounding area during the period 1986–2006, *Pure Appl. Geophys.* **124**, 597–612.
- Papazachos, B. C., B. E. Karakostas, Ch. Papaioannou, C. B. Papazachos, and E. Scordilis (1997a). A catalogue for the Aegean and surrounding area for the period 550BC–1995.
- Papazachos, B. C., A. A. Kiratzi, and B. G. Karakostas (1997b). Toward a homogeneous moment magnitude determination for earthquakes in Greece and the surrounding area, *Bull. Seism. Soc. Am.* **87**, 474–483.
- Rikitake, T. (1976). Recurrence of great earthquakes at subduction zones, *Tectonophysics* **35**, 335–362.
- Scholz, C. H. (1968). The frequency magnitude relation of microfracturing in rocks and its relation to earthquakes, *Bull. Seism. Soc. Am.* **58**, 399–415.
- Singh, S. K., L. Astiz, and J. Haskov (1981). Seismic gaps and recurrence periods of large earthquakes along the Mexican subduction zone: a reexamination, *Bull. Seism. Soc. Am.* **71**, 827–843.
- Stavrakakis, G. N. and G. A. Tselentis (1987). Bayesian probabilistic prediction of strong earthquakes in the main seismogenic zones of Greece, *Bull. Seism. Soc. Am.* **29**, 51–63.
- Wyss, M., K. Shimazaki, and S. Wiemer (1997). Mapping active magma chambers by *b*-value beneath Off-Izu volcano, Japan, *J. Geophys. Res.* **102**, 20413–20433.

Institute of Engineering Seismology and Earthquake Engineering  
(ITSAK)  
P.O. Box 53  
GR-55102, Foinikas  
Thessaloniki, Greece  
E-mail: costas@itsak.gr

Manuscript received 24 March 1998.